chemosensors

MDPI

Article

High-Performance Self-Driven SnSe/Si Heterojunction Photovoltaic Photodetector

Fuwen Luo [1], Hongxi Zhou [1,2,*], Yuxuan Liu [1], Yao Xu [1], Zhiheng Zhang [1], Chao Chen [1,2,*] and Jun Wang [1,2,*]

[1] School of Optoelectronic Science and Engineering, University of Electronic Science and Technology of China, No. 4, Section 2, Jianshe North Road, Chengdu 610054, China; luofuwen10@163.com (F.L.); 2429662l@student.gla.ac.uk (Y.L.); 13607209196@163.com (Y.X.); zhangzhihengup@163.com (Z.Z.)

[2] State Key Laboratory of Electronic Thin Films and Integrated Devices, University of Electronic Science and Technology of China, No. 4, Section 2, Jianshe North Road, Chengdu 610054, China

* Correspondence: zhouhx@uestc.edu.cn (H.Z.); chenchao@uestc.edu.cn (C.C.); wjun@uestc.edu.cn (J.W.)

Abstract: Tin monoselenide (SnSe), which belongs to group IV–VI monochalcogenides, has obtained significant attention in the field of photodetection owing to its ultrahigh carrier mobilities. However, the great challenges of preparing high-quality films and high-performance devices still need to be conquered. Herein, high-density continuous SnSe films were deposited on a Si substrate using magnetron sputtering technology, and a self-driven photovoltaic-type broadband photodetector from the visible light range (VIS) to the near-infrared (NIR) range based on SnSe/Si heterojunction was constructed. Owing to its high carrier mobility, narrow band gap structure, and strong internal electric field, the SnSe/Si heterojunction device exhibits an ultrafast response and high responsivity (R), which achieves a wide spectral response of 405–980 nm. Under zero bias voltage, the greatest R and detectivity (D*) of the heterojunction were 704.6 mA/W and 3.36 × 10^{11} Jones at 405 nm. Furthermore, the device had a fast response time (rise time) of 20.4 µs at 980 nm of illumination. This work provides a new strategy for the fabrication of high-performance, low-cost, and self-driven photodetectors.

Keywords: tin monoselenide; heterojunction; self-driven; photodetector

Citation: Luo, F.; Zhou, H.; Liu, Y.; Xu, Y.; Zhang, Z.; Chen, C.; Wang, J. High-Performance Self-Driven SnSe/Si Heterojunction Photovoltaic Photodetector. *Chemosensors* **2023**, *11*, 406. https://doi.org/10.3390/chemosensors11070406

Academic Editor: Jose Manuel Andrade

Received: 1 June 2023
Revised: 17 July 2023
Accepted: 17 July 2023
Published: 19 July 2023

1. Introduction

At present, photoelectric devices based on two-dimensional materials show excellent performance owing to their restricted dimensionality. Graphene-based photodetectors tend to detect a broadband spectrum, but the device's performance is districted owing to its low absorbance [1,2]. In contrast, photodetectors based on transition metal dihalides (TMDS) ($MoSe_2$, WS_2, and WSe_2) have remarkable photoelectric detection performance with high R [3–5]. The response wavelengths of these photodetectors are limited to visible light, and the R in the NIR region is low, which restricts their application in broadband detection. Other low-dimensional materials with narrow band gaps (<1.0 eV), such as black phosphorus (BP), have also been developed for manufacturing broadband photodetectors [6]. Nevertheless, there are some challenges in the deposition of high-quality BP films and maintaining their stability. Additionally, the large-scale preparation of BP films that are compatible with CMOS technology for focal plane array (FPA) photodetectors is not yet feasible.

Compounds in the IV–VI main group exhibit better photoelectric properties due to their smaller band gaps and high carrier mobility. Tin selenide, as a typical IV–VI main group metal–chalcogenide compound, has all the advantages of IV–VI metal–chalcogenide compounds [7]. Its band gap ranges from 0.9 eV to 1.3 eV, which makes it attractive in the application of wideband photodetectors. SnSe has high chemical stability, which enables it to maintain good performance in harsh environments (such as strong acid and alkali environments). Its natural content is not as rare as transition metals and can be

found in large natural reserves; therefore, the cost is relatively low. Photoelectric devices fabricated via SnSe have important practical applications. SnSe not only exhibits excellent photoelectric performance due to its high absorption coefficient of 10^5 cm^{-1} [8], but also has significant anisotropy and excellent thermoelectric performance. These good properties mean that tin selenide materials can be widely used in photoelectric devices. In a report on high-performance optoelectronic devices based on SnSe, the photoresponsivity of the flexible SnSe photodetector prepared by Xu reached 0.16 AW^{-1} under mid-infrared light of 10.6 μm [9], and the response speed was fast, whereas the SnSe/GaN heterojunction device prepared by Pargam Vashishtha had a high response rate and wide detection range [10]. In addition, some self-driven heterojunction detectors have been reported to have a high detector rate and wide spectral detection. A photodetector based on an exfoliated α-In_2Se_3/Ta_2NiSe_5 heterojunction can work both in a self-driven state and a bias voltage state [11]. In the self-driven state, the responsivity of the photodetector is 12 A/W and the detectivity is 3.7 × 10^{13} Jones at 520 nm. The detection spectral band covers 405 nm to 1550 nm, and the response time (rise time) is only 25 μs. The photovoltaic photodetector based on the tin selenide semiconductor exhibits excellent optical detection performance, including a rapid optical response speed. Furthermore, photovoltaic detectors can operate without bias voltage, which results in lower power consumption. This makes them suitable for the more demanding conditions of next-generation optoelectronic devices [12–14]. Moreover, SnSe film can be grown steadily and uniformly over a large area by using existing film preparation technology, and the preparation process is simple and controllable, which gives it great practical application prospects in the field of large field photodetector arrays [15,16].

Research on SnSe detectors should first focus on the controllable preparation of thin films and then study the optical detection performance of the device on the basis of the controllable preparation of thin film materials. In the existing preparation methods, Sn^{2+} in the precursor is often oxidized into Sn^{4+} during the preparation process, which is easy to lead to $SnSe_2$ instead of SnSe. Therefore, how to prepare pure-phase SnSe is an important problem. The existing methods for preparing SnSe films include evaporation, chemical vapor deposition (CVD), the sol-gel method, ion-assisted deposition, magnetron sputtering, etc. Among these methods, SnSe thin films prepared by the magnetron sputtering method have the advantages of a simple process, stable and controllable film growth, high-quality film growth, a large preparation area, and high repeatability. It has practical application prospects in the field of wide-spectrum fast-response photodetectors, which makes it particularly suitable for industrial production.

Herein, high-quality continuous and large-size SnSe films are grown on n-Si substrate using magnetron sputtering technology. The prepared SnSe film can be used for large area preparation and wafer size, with a simple process, strong controllability, and high repeatability. Additionally, SnSe/Si heterostructure photodetectors are capable of efficiently capturing VIS-NIR (405–980 nm) radiation. The device exhibits excellent photoelectric performance under zero bias voltage, with a high responsivity (R) of 704 mA/W and detectivity (D*) of 3.36 × 10^{11} Jones at 405 nm. Moreover, swift responses of 304 μs in the NIR region and 20.4 μs in the VIS region were achieved at room temperature. Therefore, this provides a new scheme for energy-efficient, sensitive photoelectric devices.

2. Materials and Methods

SnSe films are grown on (100)-oriented Si substrates via the magnetron sputtering technique method. The Si substrates are n-type semiconductors with a thickness of approximately 200 μm, a size of 1.5 × 1.5 cm, and a resistivity ranging from 1 to 10 Ω cm. The substrates are immersed in HF solution (~15%) for 30 s to eliminate the natural oxide layer from the surface of the Si substrate. Furthermore, the substrates are immersed in deionized water and undergo ultrasonic cleaning for 10 min to remove surface dust, before undergoing anhydrous ethanol and acetone ultrasonic cleaning for 15 min to remove organic impurities on the surface of the substrate. Then, they are subjected to ultrasonic cleaning

with ultra-pure water for 10 min to remove the cleaning solvent remaining on the surface of the substrate during the above cleaning process.

N_2 is used to dry the substrates, which are then secured to the substrate tray and transferred to the sputtering cavity. Mechanical pumps and molecular pumps are used to vacuum the sputtering cavity to keep the pressure at 8×10^{-4} Pa. Then, high-purity argon is used to flush the sputtering system to eliminate the pollution of other gases in the cavity. By optimizing the sputtering time, gas pressure, and sputtering power, high-quality films are obtained.

Prior to film deposition, a 10-min pre-sputtering operation is performed to avoid the impact of natural oxides and pollutants on the surface of the target on the quality of the sputtered film. Then, the formal sputtering begins to deposit the film onto the substrate. During the sputtering process, the pressure in the cavity is maintained at 0.5 Pa, the sputtering power is 16 W, and the rate of argon gas is 27.5–28.5 ccm. After the sputtering is completed, high-quality SnSe film is obtained. The SEM image shows the high continuity of the film (Figure 1a,b) in a large area.

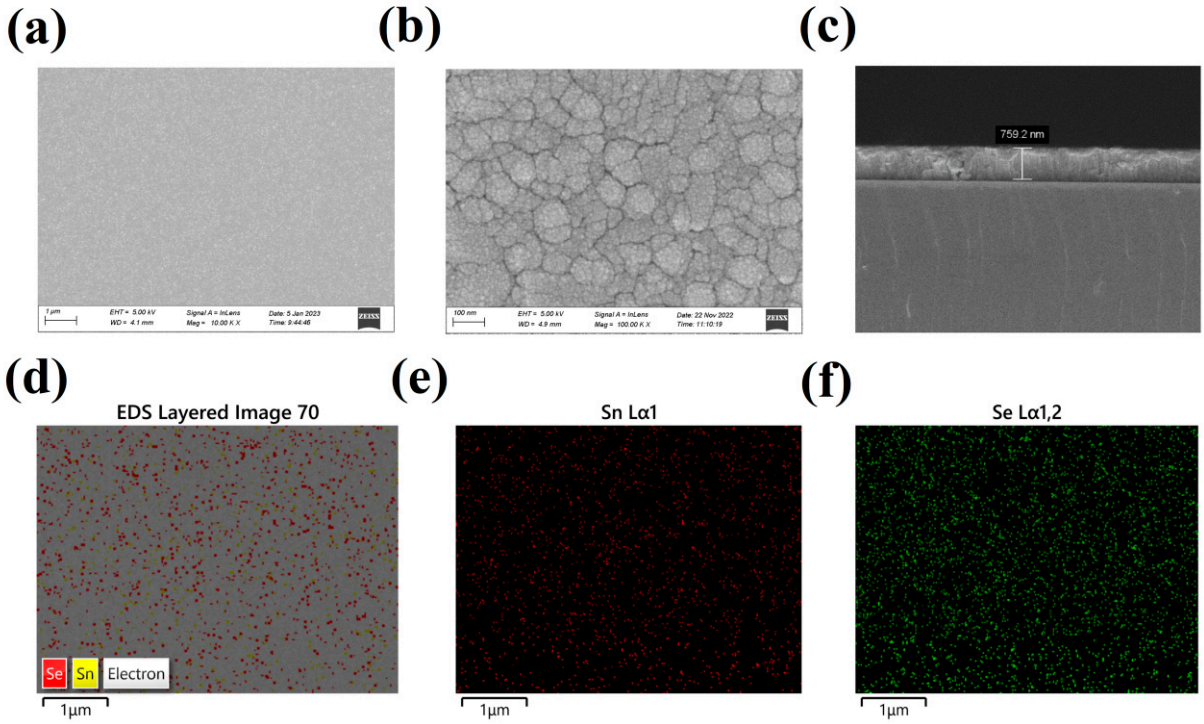

Figure 1. The structural characterization of SnSe film. (**a**,**b**) SEM image of SnSe film. (**c**) Cross-section SEM image of SnSe film. (**d**–**f**) SEM−EDS mapping of Sn and Se in the film.

The Raman spectrum test adopts Horiba LabRAM HR Evolution equipment from Japan. The wavelength of the test laser is 514 nm, and the range of the test wave numbers is 500–4000 cm^{-1}. For scanning electron microscopy (SEM), we use a GeminiSEM 300 instrument produced by the ZEISS Company in Germany to observe the surface morphology of the film and analyze the morphology characteristics of the film at different magnifications.

To fabricate the SnSe photodetector, a metal mask plate is utilized for the thermal evaporation of Au onto the surface of the SnSe film. The Au material used for electrode preparation is gold wire with a gold content greater than 99.99%. The designed metal mask is pasted onto the surface of the thin film, and the Au is steamed to the surface of the thin film using thermal evaporation equipment to prepare the shape of the target electrode. The thickness and diameter of the Au electrode are 120 nm and 1 mm, respectively. Additionally, a conductive ITO is pasted onto the back of the film and affixed with conductive silver adhesive, serving as the back electrode. The size of the ITO glass is 2 × 2 cm, and the surface conductivity is good. The silicon wafer coated with SnSe film is glued onto the

surface of the ITO using the conductivity of conductive silver glue, and the conductive silver glue is heated on the heating table for 15–20 min until completely solidified, thus forming a simple heterojunction device.

3. Results and Discussion

Figure 1a,b show the SEM image of the SnSe film growing on a silicon substrate. Figure 1a is the surface topography of the film magnified at 10 k (k means the image is magnified 1000 times). It can be observed that the surface gray level of the film image is uniform, indicating that the film has high density and uniform growth. Figure 1b is the surface topography of the film magnified at 100 k. The materials are lumpy and stacked together, and the block diameter is about 100 nm. We cut the film with a silicon knife and then analyzed the thickness of the film by looking at cross-section images. Figure 1c shows the cross-section morphology of the film with a thickness of 759.2 nm. It can be seen that the thickness of the film is uniform everywhere, and the boundary between the film and the silicon wafer substrate is obvious. Energy-dispersive spectroscopy (EDS) equipment is used to study the chemical composition of the film. It can be seen from Figure 1d that both elements exist and are evenly distributed in the film, and Figure 1e,f describe the distribution of Sn and Se in the film, respectively.

As shown in Figure 2a, the SnSe structure is an orthogonal layered structure, and the adjacent layers are connected by weak van der Waals interactions. Grazing angle X-ray diffraction and Raman spectroscopy are carried out to confirm the phases and the purity of the SnSe film. The Raman spectrum of the film is depicted in Figure 2b. The presence of peaks at 67 cm^{-1}, 106 cm^{-1}, 128 cm^{-1}, and 154 cm^{-1} can be assigned to the out-of-plane vibrations of Ag^1, Ag^2, and Ag^3, respectively. Meanwhile, the peak at 106 cm^{-1} corresponds to the in-plane vibration of B^3g [17,18]. The X-ray diffraction (XRD) spectra of the SnSe film are shown in Figure 2c, with peaks at 15.2°, 30.3°, 46.9°, and 64.2°, corresponding to the (200), (400), (600), and (800) planes of orthorhombic SnSe, respectively. The comparison with the reported literature [19] proves that we generated high-purity SnSe films. Furthermore, X-ray photoelectron spectroscopy (XPS) measurement spectra are presented in Figure 2d–f. XPS can characterize the surface elements and their chemical states. The basic principle is to use an X-ray, interact with the sample surface, use the photoelectric effect, stimulate the sample surface to emit photoelectrons, use the energy analyzer, measure the photoelectron kinetic energy, according to E(b) = hv-E(k)-W, and then obtain the binding energy of excited electrons E(b). Where E(b): binding energy, hv: photo energy, E(k): kinetic energy of the electron, and W: spectrometer work function. The peaks in the spectrum mainly arise from the Sn and Se elements. In addition, the spikes in elements C and O may be attributed to the gas molecules absorbed by the surface of the film. In Figure 2f, Se $3d_{5/2}$ and Se $3d_{3/2}$ peaks are observed at 53.2 eV and 53.8 eV, respectively, confirming the presence of Se $3d_{5/2}$ and Se $3d_{3/2}$ in the film. The XPS peaks are 485.3 eV and 493.7 eV (Figure 2d), corresponding to Sn $3d_{5/2}$ and Sn $3d_{3/2}$ [20], while the peaks at 494.7 eV and 485.4 eV result from the oxidation of tin oxide on the surface of the film [21]. During the process of film deposition, the working gas in the vacuum chamber is maintained in a high vacuum state with high purity. However, there might be oxygen molecules present, and the oxidation state in the film may be influenced by the gas molecules absorbed by the surface of the film.

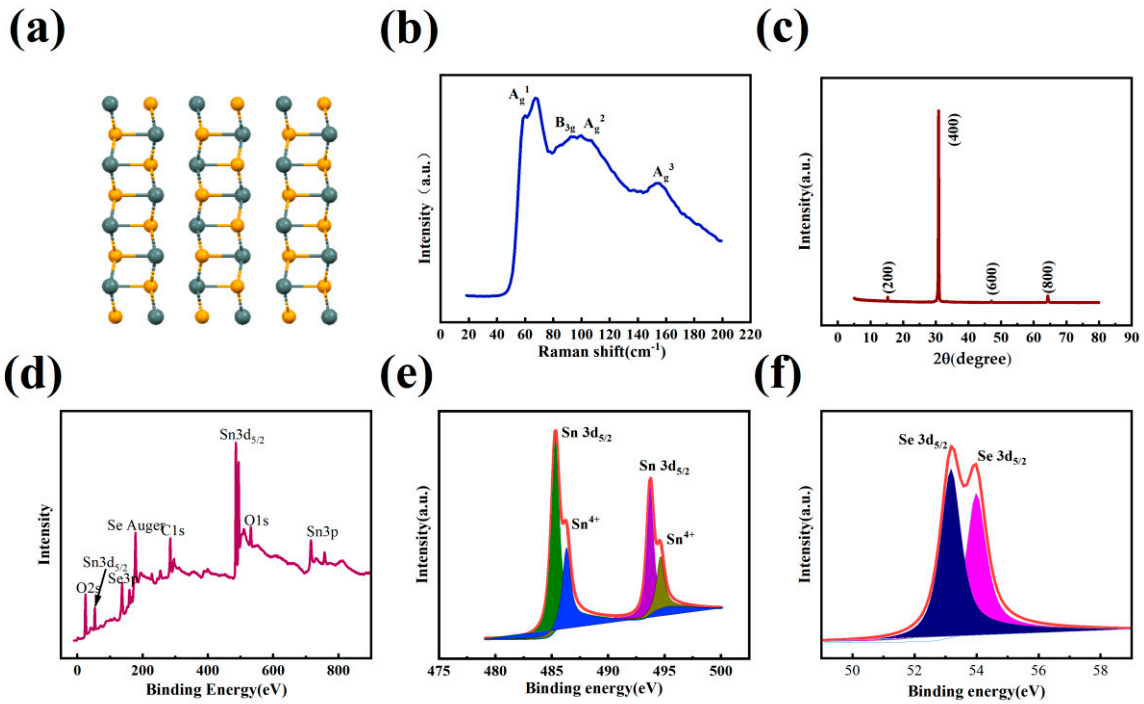

Figure 2. Microstructure of SnSe film. (**a**) SnSe crystal structure. (**b**) Typical Raman spectrum of the SnSe thin film. (**c**) XRD spectra of SnSe film. (**d**–**f**) XPS survey spectrum of the SnSe film.

Heterojunction devices exhibit self-actuated optical response characteristics, as demonstrated in the enlarged diagram of Figure 3a. Additionally, it clearly indicates that under lighting conditions, the IV curves pass through the fourth quadrant and show an obvious photovoltaic response. In other words, when the device is under zero bias, the photogenerated electron–hole pairs will rapidly separate into different material layers driven by the built-in potential. These accumulated electrons and holes disrupt the thermal balance in the dark state, resulting in a positive open-circuit voltage. When the device is short-circuited, the separated photogenerated carriers recombine and produce a short-circuited current (I) in the channel. Due to the good rectification characteristics and low reverse current of heterojunction, the photoelectric detection performance of self-driven heterostructures is studied in this paper. Furthermore, as illustrated in Figure 3b, by adding a voltage varying from −3 V to 3 V at both ends of the electrode, we scan the IV characteristic curve of the device and change the incident light intensity of the device so that we can see the change in the IV curve with the change in the incident light intensity. When the incident laser is irradiated on the heterojunction surface, the photogenerated electron–hole pairs will quickly separate and transfer to different material layers under the action of the built-in electric field. These charge carriers will transport laterally between the electrodes and contribute additional photocurrent. When the voltage (V_0) is greater than 0 V, a large number of free carriers will contribute a large forward current through the heterojunction, while the photogenerated electron–hole pairs only account for a small part, resulting in a low optical switching ratio. On the contrary, when $V_0 < 0$ V, the device works in the cutoff state, and the photogenerated electron–hole pair serves as a conductive carrier in the channel, leading to a much higher photocurrent than the dark current and thus, a high light switching on–off ratio. This demonstrates the high sensitivity of the photodiode device.

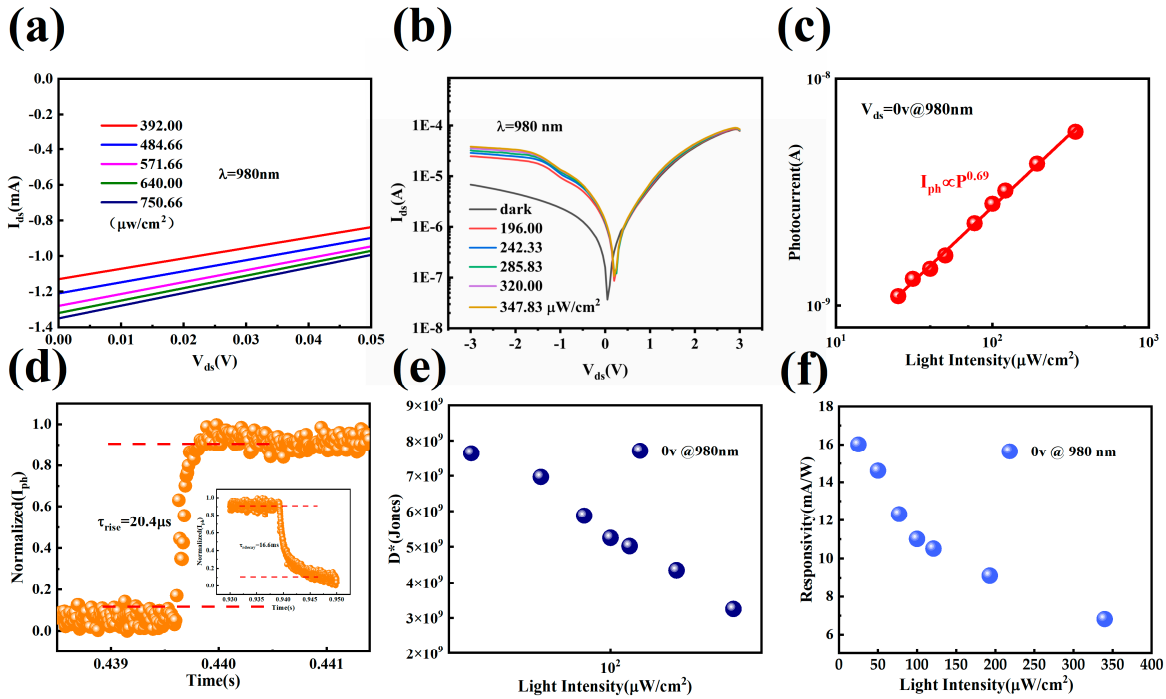

Figure 3. The detector performance of the device at 980 nm. (**a**) Enlarged $I_{ds}-Vds$ measurements under 980 nm. (**b**) IV characteristic curve of device at different laser power incidences. (**c**) Fitting curve of photocurrent variation with light intensity at 980 nm band. (**d**) Response time of 980 nm band device. (**e**) The D* of 980 nm band varies with incident light power. (**f**) Image of device responsivity variation with incident light power at 980 nm laser.

From Figure 3c, it can be seen that the trend of I_{ph} as a function of light intensity follows the power-law $I_{ph} \propto P^{\theta}$. The photocurrent strongly depends on the light intensity, where γ represents the response of I_{ph} to increasing light intensity. In an ideal heterojunction without trap states, $\theta = 1.0$. However, θ values are generally much smaller in the reported layered structured film/Si heterojunctions due to the large number of localized states between the Fermi level and the conduction band. These localized states are caused by random crystallization and poor interfaces. Here, the value of the θ index can be obtained via the linear fitting method on a logarithmic scale, where the value of $\theta \approx 0.69$. In addition, the current variation curve of a single periodic response signal after normalization with time is shown in Figure 3d, the rise time of the light response is 20.4 μs, and the decay time is 16.6 ms. This device has a fast optical response speed. This is due to the fact that the carrier drift time of photovoltaic detectors is shorter than that of photoconductive detectors, and the strong internal electric field of Schottky heterojunction devices can accelerate the drift speed of carriers. More importantly, photovoltaic detectors can operate without bias voltage and thus have lower power consumption, which can meet the more complex conditions of the working environment of the next generation of optoelectronic devices in the future. However, the R of SnSe-based heterojunction self-driven photodetectors is relatively low, which is still far behind that of photoconductive detectors, so further research is needed.

Herein, we calculate the responsivity (R) and detectivity (D*) of heterojunction photodevices, where R is the sensitivity of the device to incident light. The formula [22] for R is as follows:

$$R = I_{ph} / \left(P_{light} \times A \right) \quad (1)$$

where A is the effective device area; it is defined as the ratio of the incident light spot area to the active area of the device. The size of the spot area of different lasers is not consistent, and the active area is defined as the area of the thin film material in the circular electrode. P_{light} is the light density on the heterojunction, and I_{ph} is the photocurrent. Moreover,

detectivity (D*) is used to describe the detection ability of the detector to the optical signal, which can be calculated using the following formula [23]:

$$D^* = R(A/2eI_d)^{0.5} \quad (2)$$

Figure 3e shows the power-dependent detection rate as a function of laser wavelength. Figure 3e also shows that the D* of the heterojunction device varies with laser power intensity under the light irradiation of 980 nm in wavelength, and the maximum D* is calculated as 7.64×10^9 Jones. Compared with the previous bands, the R of the device at this band decreases significantly. Although the absorption of the film is decreased, this SnSe/Si heterostructure photodetector is still able to achieve a maximum responsivity of 16 mA/W.

The structure diagram of the heterojunction photodetector based on SnSe/Si is shown in Figure 4a. The bottom electrode is composed of a transparent conducting ITO and a cubic SnSe single crystal along the crystal phase (100), and a ring Au electrode deposited on the surface of SnSe film constitutes the top electrode. The PDA probe platform is used to test the device. The two probes are tied to the top Au electrode and the bottom ITO conductive surface, respectively, and then the device performance is tested by adjusting the parameters. Figure 4b shows the spectral absorption of heterojunction devices in the UV−visible−near−infrared range. The absorption of the devices in this band range confirms the spectral absorption curve. The devices exhibit absorption in the range from 300 nm to 1400 nm, with the peak absorption at around 400 nm. In the actual use of laser testing, we can detect the self-driven performance of the device near 1000 nm by laser testing at zero bias voltage. However, the test performance is poor after 1000 nm because the thin film's light absorption is not enough in this band, and the photo-generated carrier concentration is not enough. Figure 4c presents that the responsivity of the heterojunction device varies with the incident light power at 405–650 nm. It can be seen that the R of the device at 405 nm achieves the highest value, which is determined by the absorption characteristics of the SnSe film. The R of the device decreases with the increase in the incident light power. This is because photoelectric detection is a process in which electrons of photosensitive materials absorb photon energy and break away from atomic bondage. The number of electrons generated is proportional to the number of incident photons, but the number of electrons in the outer layer of the photodetector atom is limited, and so is the number of electrons provided per unit time. The photocurrent is proportional to the incident power. When the incident power increases to a certain amount, the photocurrent no longer changes with the increase in the optical power. When it reaches saturation, the R will become smaller if the optical power increases again. Figure 4d shows the time-varying curve of the current of the device under different laser irradiation. The curve indicates the time-varying relationship of the photoelectric response current of the device under the saturated power output of the laser in each band. It can be seen that the photocurrent produced by the device at the 405 nm, 450 nm, 650 nm, and 980 nm laser incidents is large and similar in quantity, while the photocurrent produced by the laser incidents at 780 nm and 808nm is small, which is caused by the inconsistent saturation power of the laser. Among them, the laser power from the 405nm to 980nm band is 15.80 mW, 6.63 mW, 0.94 mW, 0.85 mW, 3.04 mW, and 23.59 mW, respectively. The function of D* and the incident power of the device at the 650 nm, 405 nm, and 450 nm band are shown in Figure 4e. It can be seen that its maximum D* is 3.36×10^{11} Jones at 405 nm, and its maximum D* is 1.07×10^{11} Jones at 650 nm. With the increase in laser density, the D* of the incident light decreases. This is because the initial incident light power is low, and the light absorbed by the thin film material is completely converted into a photocurrent. With the increase in the incident light power, the material's absorption of photon energy reaches saturation, and when the light intensity is changed, the excess energy is converted into a photothermal response. The photoelectrical response is measured, as shown in Figure 4f. Under the 405 nm illumination, the I_{ph} is increased with the increase in light intensity, and

it complies with a fitted power law equation of $I_{ph} \propto P^{0.74}$. The heterojunction device has the highest responsiveness and detection rate at 405 nm, and its exponential factor value is close to 1, showing more obvious heterojunction characteristics. The result indicates that the response mechanisms of the low light intensity region are photogating [24].

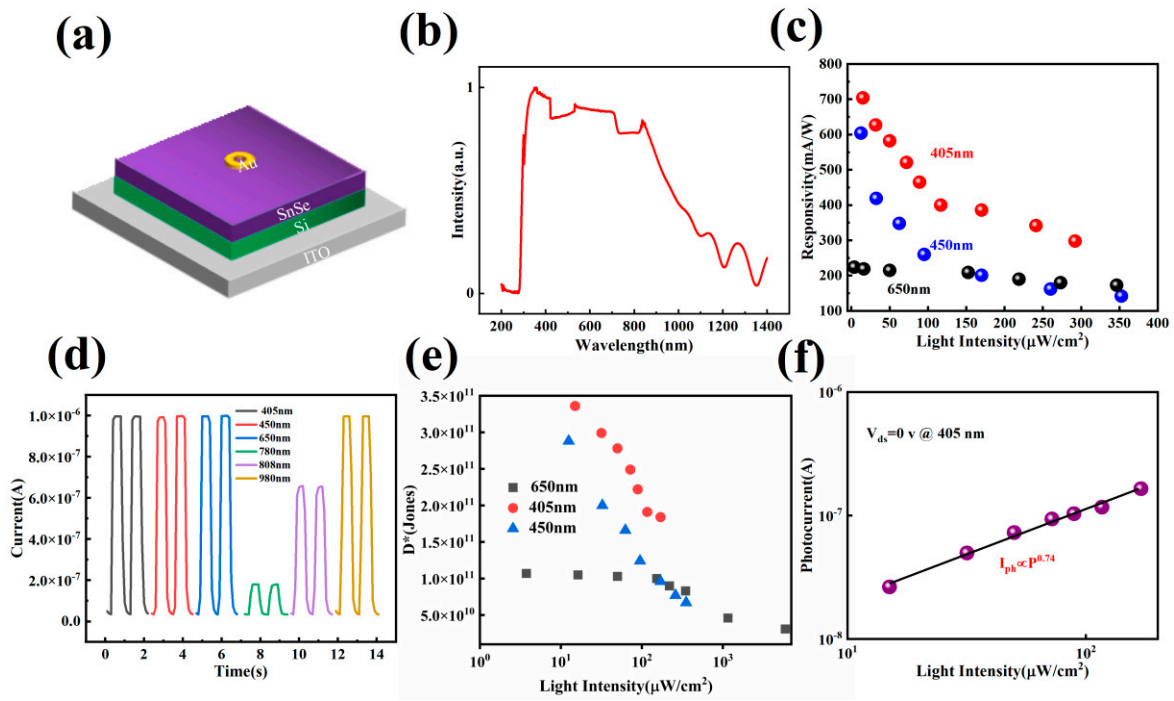

Figure 4. The device responds to light at different wavelengths. (**a**) Three-dimensional structure diagram of heterojunction device. (**b**) The spectral response of heterojunction devices in the range from 300 nm to 1400 nm. (**c**) Plots of responsivity of the heterojunction under the 405 nm, 450 nm, and 650 nm wavelengths of light illumination as a function of laser power intensity. (**d**) Devices in different wavelength IT curves. (**e**) D* variation curve with incident light intensity at 405 nm, 450 nm, and 650 nm. (**f**) The fitting curve of photocurrent with incident light intensity at 405 nm.

Table 1 summarizes other key parameters reported for the performance of two-dimensional SnSe−based photodetector devices. Among them, the heterojunction device created by Hao [25] has an excellent response speed and wide detection band. Its maximum R is 566 mA/W at 850 nm. The heterojunction device prepared in this paper improved the maximum R, which is 704.6 mA/W at 405 nm, and we did not need to heat the substrate, so the preparation power consumption was lower and the process was simpler. However, other SnSe-based photodetectors [26–29] in the table have a slow response time and low R, which cannot meet the requirements of high−speed sensitive detection. In addition, the preparation process for these optoelectronic devices is complicated, the preparation requirements are high, and the repeatability is not strong. The device prepared in this paper is far superior to the above photodetectors in terms of R and response speed. Current SnSe/Si heterojunctions exhibit a competitive electro−optical performance when operating with self-actuation at zero bias and, in particular, exhibit higher detection rates and lower response times compared to SnSe with a larger transverse size. In addition, the current photodetectors based on gallium arsenide have a wide spectrum of detection frequency bands and higher performance. The detection performance of the photodetector based on the SnSe prepared in this paper is better than that of a gallium arsenide photodetector [30] reported at present, with a higher responsiveness and lower cost. Of course, there is also room for improvement in the response speed of this device. Due to the large film area of the device growth, leakage and other factors will exert influence, resulting in a large dark current value, and the response current makes it difficult to reach a large value. The further optimization of the process to suppress the dark current level can further improve

the device's R, detection rate, and other performance indicators. Furthermore, its excellent photoelectric detection performance is mainly attributed to the following aspects: (1) SnSe has a unique and excellent crystal structure, and the interface formed between SnSe and Si can minimize the defect density in the heterojunction, thus greatly inhibiting the capture of photoexcited carriers and promoting the transport characteristics of carriers at the heterojunction. (2) The large internal electric field at the heterogeneous interface can reduce the dark current. Especially, large internal electric fields can effectively promote the separation of photoexcited electron–hole pairs and significantly shorten the transit time of photoexcited carriers.

Table 1. Photodetectors with device structure and other details reported in the literature.

Materials	Spectrum (nm)	R (A/W)	τ (μs)	Refs.
Au/SnSe/Si	300–1000	0.704	20.4	This work
Pd/SnSe/Si	300–1100	0.566	1.6	[25]
SnSe film	370–808	0.0014	178	[26]
$SnSe/In_2Se_3$	405	0.350	1.39×10^5	[27]
Gr/SnSe/Gr	100–1050	0.038	0.18×10^6	[28]
SLG/SnSe/Ag	532–1064	0.0014	5×10^3	[29]
Si/GaAs	635	0.06	none	[30]

4. Conclusions

We used RF magnetron sputtering technology to deposit SnSe films onto Si substrates. Upon optimizing the growth parameters, high-quality single−crystal SnSe films were fabricated. Additionally, a SnSe/Si unilateral Schottky heterojunction with an atomic mutation interface was then prepared, resulting in a high−performance self−driven heterojunction photodetector. The photoelectric properties of the SnSe/Si heterojunction under different irradiation wavelengths were systematically studied with a high responsivity of 704 mA/W, and the corresponding D* was 3.36×10^{11} Jones. The device had an ultra-fast response time of 20.4 μs and a wide spectral response of 405−980 nm. Compared with SnSe photoconductive photodetectors, the thin−film heterojunction photovoltaic photodetectors show a faster response and higher detection performance. In general, this work proves the high performance of SnSe/Si heterojunction photodetectors and provides a promising system for fast and high response detection in VIS−NIR spectral bands.

Author Contributions: Conceptualization, F.L., J.W., Y.X. and Z.Z.; methodology, F.L., H.Z. and J.W.; software, F.L., Y.L., Y.X., Z.Z. and J.W.; validation, F.L., H.Z. and Y.L.; formal analysis, F.L., Y.X., Z.Z. and C.C.; investigation, H.Z., C.C. and J.W.; data curation, F.L., Y.L., Y.X. and Z.Z.; writing—original draft preparation, F.L.; writing—review and editing, F.L., H.Z. and C.C.; visualization, F.L., H.Z. and Z.Z.; supervision, C.C.; project administration, H.Z., J.W. and C.C.; funding acquisition, J.W. All authors have read and agreed to the published version of the manuscript.

Funding: This work is partially supported by the National Natural Science Foundation of China (NSFC) (No. 62104026, No. 62175026) and the Natural Science Foundation of Sichuan Province (2022NSFSC0960).

Data Availability Statement: Not applicable.

Conflicts of Interest: The authors declare no conflict of interest.

References

1. Jiang, J.; Wen, Y.; Wang, H.; Yin, L.; Cheng, R.; Liu, C.; Feng, L.; He, J. Recent advances in 2D materials for photodetectors. *Adv. Electron. Mater.* **2021**, *7*, 2001125. [CrossRef]
2. Xia, F.; Mueller, T.; Lin, Y.-M.; Valdes-Garcia, A.; Avouris, P. Ultrafast graphene photodetector. *Nat. Nanotechnol.* **2009**, *4*, 839–843. [CrossRef] [PubMed]
3. Lopez-Sanchez, O.; Lembke, D.; Kayci, M.; Radenovic, A.; Kis, A. Ultrasensitive photodetectors based on monolayer MoS2. *Nat. Nanotechnol.* **2013**, *8*, 497–501. [CrossRef] [PubMed]
4. Wang, Z.; Li, Q.; Besenbacher, F.; Dong, M. Facile Synthesis of Single Crystal $PtSe_2$Nanosheets for Nanoscale Electronics. *Adv. Mater.* **2016**, *28*, 10224–10229. [CrossRef] [PubMed]
5. Zhou, X.; Hu, X.; Zhou, S.; Song, H.; Zhang, Q.; Pi, L.; Li, L.; Li, H.; Lv, J.; Zhai, T. Tunneling diode based on WSe_2/SnS_2 heterostructure incorporating high detectivity and responsivity. *Adv. Mater.* **2018**, *30*, 1703286. [CrossRef] [PubMed]
6. Guo, Q.; Pospischil, A.; Bhuiyan, M.; Jiang, H.; Tian, H.; Farmer, D.; Deng, B.; Li, V.; Han, S.-J.; Wang, H.; et al. Black phosphorus mid-infrared photodetectors with high gain. *Nano Lett.* **2016**, *16*, 4648–4655. [CrossRef]
7. Hao, L.; Du, Y.; Wang, Z.; Wu, Y.; Xu, H.; Dong, S.; Liu, H.; Liu, Y.; Xue, Q.; Han, Z.; et al. Wafer-size growth of 2D layered SnSe films for UV-Visible-NIR photodetector arrays with high responsitivity. *Nanoscale* **2020**, *12*, 7358–7365. [CrossRef]
8. Zhao, L.-D.; Lo, S.-H.; Zhang, Y.; Sun, H.; Tan, G.; Uher, C.; Wolverton, C.; Dravid, V.P.; Kanatzidis, M.G. Ultralow thermal conductivity and high thermoelectric figure of merit in SnSe crystals. *Nature* **2014**, *508*, 373–377. [CrossRef]
9. Mahjouri-Samani, M.; Gresback, R.; Tian, M.; Wang, K.; Puretzky, A.A.; Rouleau, C.M.; Eres, G.; Ivanov, I.N.; Xiao, K.; McGuire, M.A.; et al. Pulsed Laser Deposition of Photoresponsive Two-Dimensional GaSe Nanosheet Networks. *Adv. Funct. Mater.* **2014**, *24*, 6365–6371. [CrossRef]
10. Vashishtha, P.; Kumar, M.; Prajapat, P.; Ahmed, J.; Singh, V.N.; Gupta, G. Highly responsive SnSe/GaN heterostructure-based UVC-SWIR broadband photodetector. *Mater. Sci. Semicond. Process.* **2023**, *156*, 107277. [CrossRef]
11. Li, H.; Zhang, K.; Li, X.; Liu, B.; Li, L.; Mei, Z.; Chen, T.; Liu, Q.; Yu, W.; Yuan, J.; et al. Two-dimensional (2D) α-In_2Se_3/Ta_2NiSe_5 heterojunction photodetector with high sensitivity and fast response in a wide spectral range. *Mater. Des.* **2023**, *227*, 111799. [CrossRef]
12. Kang, J.; Sangwan, V.K.; Lee, H.-S.; Liu, X.; Hersam, M.C. Solution-Processed Layered Gallium Telluride Thin-Film Photodetectors. *ACS Photonics* **2018**, *5*, 3996–4002. [CrossRef]
13. Liu, J.; Li, X.; Wang, H.; Yuan, G.; Suvorova, A.; Gain, S.; Ren, Y.; Lei, W. Ultrathin High-Quality SnTe Nanoplates for Fabricating Flexible Near-Infrared Photodetectors. *ACS Appl. Mater. Interfaces* **2020**, *12*, 31810–31822. [CrossRef] [PubMed]
14. Wang, F.; Li, L.; Huang, W.; Li, L.; Jin, B.; Li, H.; Zhai, T. Submillimeter 2D Bi_2Se_3 flakes toward high-performance infrared photodetection at optical communication wavelength. *Adv. Funct. Mater.* **2018**, *28*, 1802707. [CrossRef]
15. Liu, W.; Zhu, Y.N.; Liu, M.; Wen, B.; Fang, S.; Teng, H.; Lei, M.; Liu, L.-M.; Wei, Z. Optical properties and applications for MoS_2-Sb_2Te_3-MoS_2 heterostructure materials. *Photonics Res.* **2018**, *6*, 220–227. [CrossRef]
16. Hu, X.; Wu, J.; Wu, M.; Hu, J. Recent developments of infrared photodetectors with low-dimensional inorganic nanostructures. *Nano Res.* **2021**, *15*, 805–817. [CrossRef]
17. Li, L.; Chen, Z.; Hu, Y.; Wang, X.; Zhang, T.; Chen, W.; Wang, Q. Single-Layer Single-Crystalline SnSe Nanosheets. *J. Am. Chem. Soc.* **2013**, *135*, 1213–1216. [CrossRef]
18. Zhao, S.; Wang, H.; Zhou, Y.; Liao, L.; Jiang, Y.; Yang, X.; Chen, G.; Lin, M.; Wang, Y.; Peng, H.; et al. Controlled synthesis of single-crystal SnSe nanoplates. *Nano Res.* **2015**, *8*, 288–295. [CrossRef]
19. Li, J.; Zhang, Q.; Liu, F.; Su, L.; Zhang, H. Ultrasensitive and Self-Powered SnSe/Ge Heterojunction Photodetector Driven by Spontaneously Interfacial Excitation Transfer of Carriers. *Adv. Mater. Interfaces* **2022**, *9*, 2201624. [CrossRef]
20. Yao, J.; Zheng, Z.; Yang, G. All-layered 2D optoelectronics: A high-performance UV–vis–NIR broadband SnSe photodetector with Bi_2Te_3 topological insulator electrodes. *Adv. Funct. Mater.* **2017**, *27*, 1701823. [CrossRef]
21. Modiba, F.; Arendse, C.J.; Oliphant, C.J.; Jordaan, W.A.; Mostert, L. Evolution of the chemical composition of Sn thin films heated during x-ray photoelectron spectroscopy. *Surf. Interfaces* **2019**, *17*, 100378. [CrossRef]
22. Li, F.; Chen, H.; Xu, L.; Zhang, F.; Yin, P.; Yang, T.; Shen, T.; Qi, J.; Zhang, Y.; Li, D.; et al. Defect engineering in ultrathin SnSe nanosheets for high-performance optoelectronic applications. *ACS Appl. Mater. Interfaces* **2021**, *13*, 33226–33236. [CrossRef] [PubMed]
23. Wang, H.; Zhang, S.; Zhang, T.; Liu, J.; Zhang, Z.; Yuan, G.; Liang, Y.; Tan, J.; Ren, Y.; Lei, W. SnSe nanoplates for photodetectors with a high signal/noise ratio. *ACS Appl. Nano Mater.* **2021**, *4*, 13071–13078. [CrossRef]
24. Zhou, H.; Liu, S.; Yang, M.; Liu, X.; Zhang, X.; Zhou, X.; Han, J.; Gou, J.; Wang, J.; Jiang, Y. Flexible Sb0.405Te0.595 photodetectors with broadband spectral response up to 4.5 μm. *Acta Mater.* **2022**, *226*, 117631. [CrossRef]
25. Hao, L.; Wang, Z.; Xu, H.; Yan, K.; Dong, S.; Liu, H.; Du, Y.; Wu, Y.; Liu, Y.; Dong, M. 2D SnSe/Si heterojunction for self-driven broadband photodetectors. *2D Mater.* **2019**, *6*, 034004. [CrossRef]
26. Ramasamy, P.; Manivasakan, P.; Kim, J. Phase controlled synthesis of SnSe and $SnSe_2$ hierarchical nanostructures made of single crystalline ultrathin nanosheets. *CrystEngComm* **2015**, *17*, 807–813. [CrossRef]
27. Li, X.Z.; Wang, Y.F.; Xia, J.; Meng, X.M. Growth of vertical heterostructures based on orthorhombic SnSe/hexagonal In 2 Se 3 for high-performance photodetectors. *Nanoscale Adv.* **2019**, *1*, 2606–2611. [CrossRef]

28. Zhong, Y.; Zhang, L.; Sun, M.; Wang, M.; Chen, W.; Lin, S.; Xie, D.; Zhu, H. Large scale self-assembly of SnSe nanosheets prepared by the hot-injection method for photodetector and capacitor applications. *Mater. Today Energy* **2019**, *12*, 418–425. [CrossRef]
29. Kumar, M.; Rani, S.; Vashistha, P.; Pandey, A.; Gupta, G.; Husale, S.; Singh, V. Low bias operated, fast response SnSe thin film Vis-NIR photodetector on glass substrate using one-step thermal evaporation technique. *J. Alloys Compd.* **2021**, *879*, 160370. [CrossRef]
30. Kim, S.H.; Geum, D.M.; Park, M.S.; Kim, H.; Song, J.D.; Choi, W.J. Fabrication of high-quality GaAs-based photodetector arrays on Si. *Appl. Phys. Lett.* **2017**, *110*, 153505. [CrossRef]